Project Report
NOAA-28

GOES Advanced Baseline Sounder (ABS)
Design Changes for Improved Spatial Performance

M.E. MacDonald
E.C. Wack
M. Kelly
D.P. Ryan-Howard

2 March 2000

This work was sponsored by the National Oceanic and Atmospheric Administration under U.S. Air Force Contract F19628-95-C-0002.

ABSTRACT

This report documents a series of design changes made to the Advanced Baseline Sounder (ABS) point design[1] formulated by MIT Lincoln Laboratory in January of 1999. These design changes were undertaken at the request of NOAA after it was recognized by NESDIS personnel that the January, 1999 ABS point design had a degradation in spatial response characteristics compared to the GOES I-O filter-wheel sounder. Implementation of the design changes set forth in this document produce an ABS point design which equals the spatial performance of the filter-wheel sounder with regard to ensquared energy. This modified point design is expected to exceed the performance of the filter-wheel sounder with regard to immunity from cloud contamination.

These design changes do not introduce elements of technical risk not present in the January, 1999 ABS point design, nor do they degrade the accuracy of retrieved soundings beyond the thresholds to which ABS was designed.

[1] L. Candell, et. al, "Advanced Baseline Sounder Design Study," Project Report NOAA-24, MIT Lincoln Laboratory, 28 January, 1999.

ACKNOWLEDGMENTS

The authors gratefully acknowledge Monica Coakley and Harry Finkle for providing retrieval error estimates. We are also grateful to Karen Hovsepian for her assistance in preparing the manuscript.

We are indebted to Paul Menzel of the NOAA/NESDIS Office of Research and Applications for motivating this work and guiding it throughout its evolution.

TABLE OF CONTENTS

LIST OF ILLUSTRATIONS

LIST OF TABLES

1. OVERVIEW

This document serves as an addendum to the Advanced Baseline Sounder design study[2]. It examines the spatial performance of the baseline design, and presents design modifications intended to produce spatial performance comparable to the existing filter-wheel GOES sounder.

1.1 BACKGROUND AND MOTIVATION

The motivation for this white paper were discussions with members of the GOES sounding community[3] who noted that the ABS design documented in reference (1) had reduced spatial resolution compared with the existing sounder, and who sought to avoid any such reductions in the instrument point-design released to industry. The remainder of this document addresses these concerns through changes to the ABS design. Implementation of these design changes is expected to increase the ensquared energy of ABS to equal that of the GOES I-M sounder, while improving its ability to obtain accurate clear-air soundings in the vicinity of cloudy regions.

1.2 SUMMARY OF RECOMMENDED DESIGN CHANGES

As a result of the analyses detailed in Section 3, MIT Lincoln Lab recommends that the following changes be made to the baseline ABS design of reference (1):

1. The ABS aperture should be increased in diameter from 15.2 cm to 25.4 cm.

2. The ABS focal plane should be reconfigured from abutted 60-μm pixels to 48-μm pixels spaced at a 60-μm pitch.

3. A neutral-density spatial filter (apodizing filter) should be inserted at the pupil located at the LWIR detector cold stop.

   The first two design changes are sufficient to equalize the spatial performance of ABS to that of the GOES I-M sounder. The third is expected to improve the immunity of ABS to "cloud contamination", representing an improvement in performance over the GOES I-M sounder. The following changes flow down from the three above.

4. The array format changes from 16 x 16 pixels to 13 x 13 pixels in all channels.

5. The instrument volume estimate changes from 0.6 x 0.7 x 0.6 meters to 0.6 x 0.8 x 0.8 meters.

6. The instrument mass estimate changes from 77 kg to 107 kg

7. The instrument power consumption estimate changes from 70 W to 90 W (assuming item #8).

[2] L. Candell, et. al, "Advanced Baseline Sounder Design Study," Project Report NOAA-24, MIT Lincoln Laboratory, 28 January, 1999.
[3] Paul Menzel, NOAA/NESDIS Office of Research and Applications, private communications with MIT/LL staff.

8. The scan mirror construction changes from a 50% lightweighted aluminum structure to a lightweighted-beryllium structure such as that used on the GOES I-M sounder.

The resulting point design is summarized in Section 2.

2. REVISED ABS POINT DESIGN

This section presents a brief overview of the December, 1999 ABS point design. The information in Table 1 is repeated from Reference (1), which presented the January, 1999 point design, and reflects changes described in this document.

The design changes investigated in this work do not introduce elements of technical risk not present in the original ABS design, nor do they achieve better spatial performance by degrading performance in other areas beyond the NWS threshold levels. Under any combination of the above three measures investigated in this work, ABS remains a design which brings about a dramatic improvement in the sounding capabilities available from geosynchronous orbit while remaining smaller, and lighter than the existing GOES sounder.

Radiometric simulations of the point design, illustrated in Figure 1, indicate that the performance is adequate to ensure the observational accuracy of retrieved soundings, as shown in Figure 2.

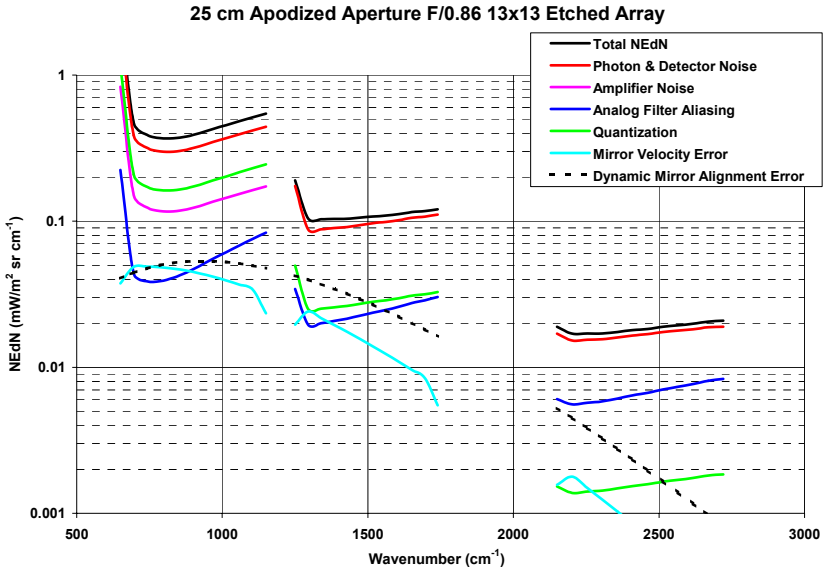

Figure 1. The modeled radiometric performance of the ABS point design is illustrated.

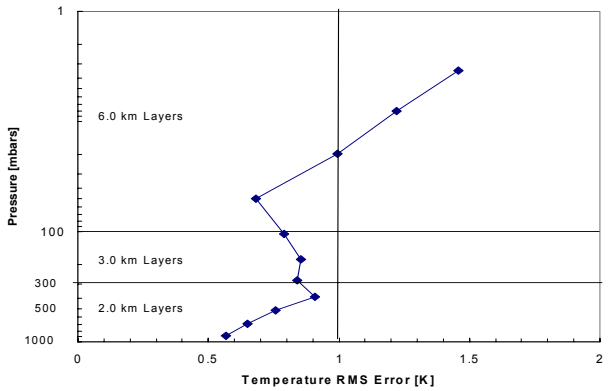

Figure 2. The modeled temperature-retrieval accuracy of the ABS point design is illustrated.

TABLE 1

ABS Instrument Summary

Feature	Description
Optical aperture	25.4 cm (10 in)
Scan method	2-axis, step & dwell, 3.6 mrad (130 km SSP) steps, E-W & N-S
Dwell time	2.0 s
Coverage rate	3000 km (N-S) x 5000 km (E-W) in 30 min
Spatial resolution	278 μrad full-angle (10 km, SSP)
Spectral resolution	2.5 cm^{-1}, 2150 – 2720 cm^{-1} (shortwave)band 1.25 cm^{-1}, 1210 – 1740 cm^{-1} (midwave)band 0.625 cm^{-1}, 662 – 1150 cm^{-1} (longwave)band
Input telescope	Three-mirror, re-imaging, afocal telescope
Interferometer	Michelson interferometer, 2.8 cm diameter, ZnSe beamsplitter, porch-swing moving mirror in one arm, dynamically-aligned mirror (error < 0.8 μrad) in second arm
Interferometer mirror sweep	± 0.4 cm, RMS velocity fluctuation < ±1%
Aft-optics	Catadioptric, field-imaging, *f*/0.85 optics
Visible channel	Silicon 260 x 260 CCD, 12 μm pixels, 300 K operating temperature, 14 μrad pixel FOV (0.5 km, SSP), SNR = 600 for 10 ms integration
Star sensing	SNR ≥ 6 for B0-class star
Data output	14-bit quantization
Data rate	~2.5 Mbit/s
Detector focal planes (all bands, unless otherwise noted)	PV HgCdTe 13 x 13 arrays, 48 μm wide pixels on 60 μm pitch, 75 K operating temperature, 278 μrad pixel FOV (10 km, SSP), 115 μs integration time (8.6 KHz frame rate), single 1.5 Mpix/s output, 2.8 x 10^8 e^- charge storage. λ_{cutoff} = 4.7 μm , SW band λ_{cutoff} = 8.0 μm, MW band λ_{cutoff} = 15.1 μm, LW band
Passive cooler construction	Three-stage design, no sun shield, ε = 0.90 EOL, 75 K patch (control point for IR detectors) 125 K radiator 220 K housing (control point for cold optics)
Passive cooler thermal budget (non-parasitic)	30 mW dissipation for each of three IR FPA's @ 75 K, 10 mW conduction to patch through wires, 60 mW control power to patch heaters. 15 W optics dissipation to housing @ 220 K
Passive cooler stage area	Patch: 1310 cm^2, Radiator: 280 cm^2, Housing: 1320 cm^2 Overall size of square cooler ≈ 64 cm x 64 cm
Calibration intervals	Space view: TBD, Blackbody view: TBD
Internal calibration blackbody	T = 320 K assumed in modeling
Predicted channel NEdN	0.02 mW/(m^2 sr cm^{-1}), SW band 0.10 mW/(m^2 sr cm^{-1}), MW band 0.40 mW/(m^2 sr cm^{-1}), LW band
Predicted retrieval accuracy	surface-300 mb: ≤ ± 1.0 K, ≤ ± 10% rel. humidity 300-100 mb: ≤ ± 1.0 K, ≤ ± 20% rel. humidity above 100 mb: ≤ ± 1.0 K
Instrument power consumption	~ 90 W
Instrument mass	~ 110 Kg
Instrument dimensions	0.6 x 0.6 x 0.8 m (not including electronics)

3. ABS INSTRUMENT SPATIAL RESPONSE, AND DESIGN OPTIONS FOR IMPROVING IT

We have chosen to define the instrument spatial response[4] in earth-scene coordinates, as this is more convenient for the users of the data. We bear in mind, however, that the physical processes governing the ABS spatial response occur with reference to the focal plane.

3.1 SPATIAL-RESPONSE LIMITATIONS OF THE JANUARY, 1999 ABS DESIGN

In Figure 3a, the spatial response of the January, 1999 ABS design is shown at λ = 15 μm. This design used a 15.2-cm aperture diameter. Since the detector had been designed to cover a 10-km (geometric) FOV, the spatial response has a half-width equal to 10 km. The diameter of the diffraction spot at the first null is 8.7 km, which is sufficiently large that the ensquared energy from the ground FOV falls below the 80% level. The corresponding spatial response of the GOES I-M sounder is shown in Figure 3b, illustrating the use of an 8-km detector width and the smaller diffraction spot obtained with this instrument's 30-cm aperture diameter. It is readily apparent from Figure 3b that the ensquared energy for a 10-km FOV is substantially larger than that of Figure 3a.

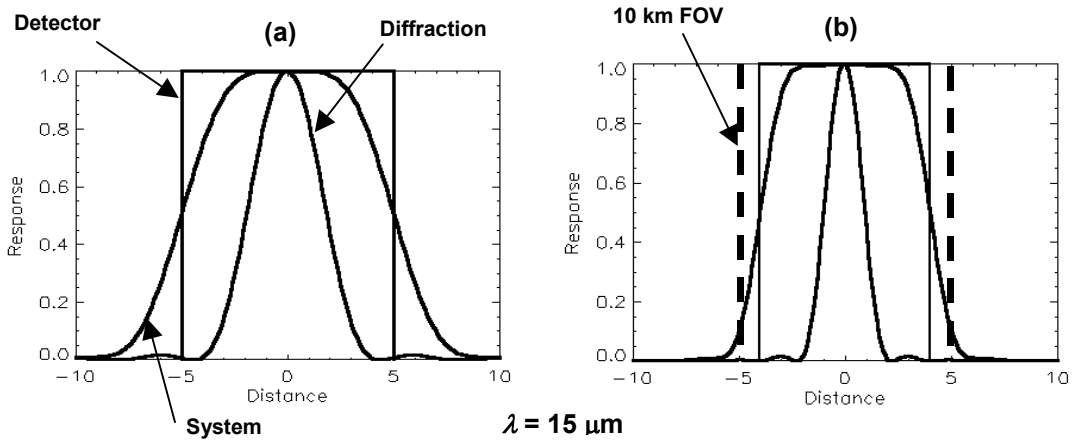

Figure 3. The spatial response of the January, 1999 ABS design is shown at left, while that of the GOES I-M sounder is shown at right.

The radiometric implications of the differing spatial responses of 15-cm and 30-cm apertures are illustrated in Figure 4, where the measured radiance at λ = 14 μm obtained in the center of a 30 x 30-km cloudless region (T_B = 290 K) within an extended cloudy background (T_B = 60 K) is shown. The central 10 x 10-km FOV of this cloudless region is subject to radiance errors arising from the degraded spatial response associated with a 15-cm aperture diameter versus a 30-cm aperture diameter. For comparison, the detector size of both cases is assumed to be 8 km.

[4] See Appendix A for a definition of the terms used in this document.

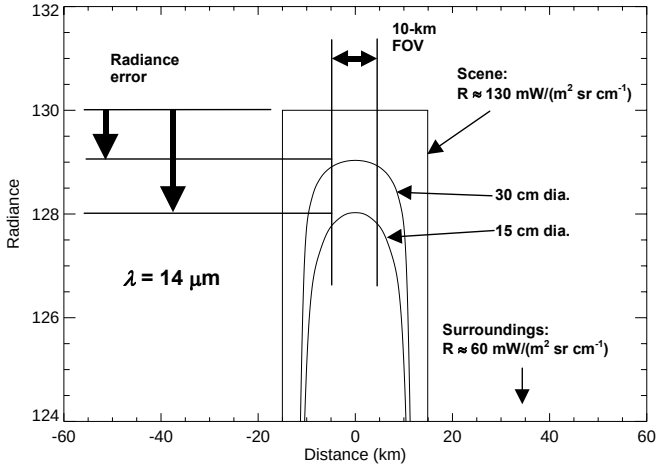

Figure 4. The radiance error produced by the increased diffraction spot diameter associated with a 15-cm aperture versus that of a 30-cm aperture is illustrated for the case of sounding in the center of a 3x3 FOV "clear" region surrounded by a cloud-covered region.

In order to equalize the spatial performance of the January, 1999 ABS design to that of the GOES I-M sounder, one obvious approach is to increase the 15-cm diameter to approach the 30-cm diameter of the I-M sounder. The effect of this design change is illustrated in Figure 5, which demonstrates that this alone is not sufficient to equal the performance of the I-M sounder, unless the detector size (e.g. the focal-plane fill factor) is reduced. In a design like ABS where an imaging array is used, it is preferred that FOV's be contiguous. The I-M sounder uses four FOV's which are not contiguous, hence the 8-km detector size is not constrained to be matched to the 10-km ground FOV. The benefit of undersizing the detector is illustrated in Figure 5. This figure demonstrates that a combination of detector size reduction and aperture diameter increase permit ABS to duplicate the ensquared energy of the GOES I-M sounder. A more detailed study of these design changes to ABS is explored in Section 3.2.

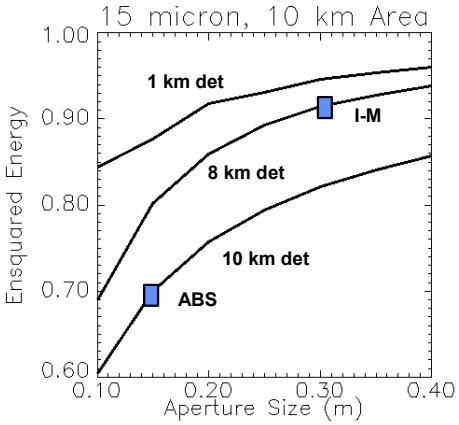

Figure 5. The parametric dependence of ensquared energy on detector size and aperture diameter is illustrated for three detector sizes, explaining the difference in performance between the January, 1999 ABS design and the GOES I-M sounder.

What is not illustrated directly in Figure 5, but is clear from Figure 4, is that the effects of diffraction are not confined exclusively to *adjacent* fields of view, but cause contamination of clear-air soundings from cloudy backgrounds several FOV's away. Measures which may be taken to diminish the diffraction rings which give rise to this phenomenon are discussed in Section 3.3.

3.2 EFFECTS OF INCREASED APERTURE DIAMETER AND DECREASED DETECTOR SIZE ON ABS SPATIAL PERFORMANCE

As previously described, modifications to the ABS instrument aperture diameter and the detector size are required in order to equalize the spatial performance of this design to that of the GOES I-M sounder. The scope of this effort was to investigate the effects of these adjustments without changing the fundamental instrument design. For this reason, the following constraints were imposed on the design alterations:

1. The detector pixel charge storage capacity was held constant at the 60 μm pixel-width value (2.8 x 10^8 e^-).

2. The readout rate was held constant at 1.5 Mpix/sec, corresponding to a single output.

3. The interferometer diameter was held constant at 2.8 cm (1.1 inches).

These constraints ensured that the ABS design downstream from the telescope (e.g. interferometer, aft optics, detector temperatures and passive cooler) remained unchanged except for minor adjustments to the size and figure of the optics. The alterations to the ABS design mean that appreciable changes may be anticipated in the following parameters:

1. The instrument volume and mass are expected to increase proportionally to the aperture diameter, since these quantities are heavily dependent on the input telescope and scan mirror.

2. The detector array size (number of pixels) is expected to change so that a single output may still be used in the presence of increased photocurrent.

3. The system NEdN is expected to degrade somewhat with smaller detector size and/or the use of an apodizing filter, although the increased aperture largely offsets this.

4. The wavelength-sensitivity of instrument spatial response is expected to increase, also as a result of smaller detector size (in Figure 3 one can verify that as the detector size decreases, the system spatial response converges to the wavelength-dependent diffraction spot).

3.2.1 Optical Designs for 20-cm and 25-cm Aperture Diameters

In order to verify that the ABS instrument aperture can be increased with only minimal changes to the interferometer and aft optics, two new optical designs were generated with 20.3 cm and 25.4 cm aperture diameters. Optical simulations indicate that both perform satisfactorily, and the resulting input telescope sizes can be used to estimate the volume and mass increases associated with the increased aperture. The optical layouts of the 15- 20- and 25-cm aperture systems are shown in Figures 6, 7, and 8 respectively.

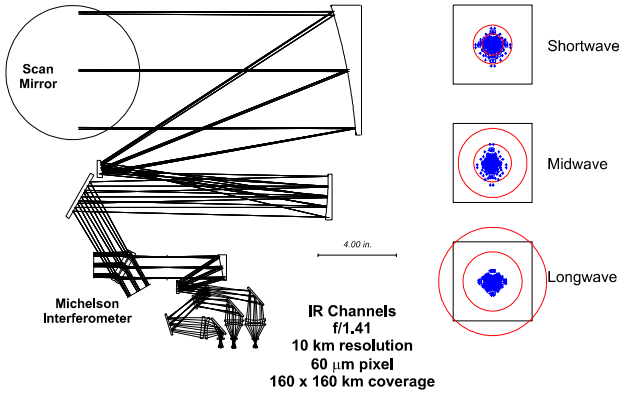

Figure 6. The optical layout of the ABS system is shown for a 15.2 cm aperture diameter. The scale bar corresponds to 10.16 cm (4 inches). Spot diagrams at the right side show the optical performance for each of the three wavebands (the circles correspond to the first two nulls of the Airy pattern, the squares represent the 60 μm detector).

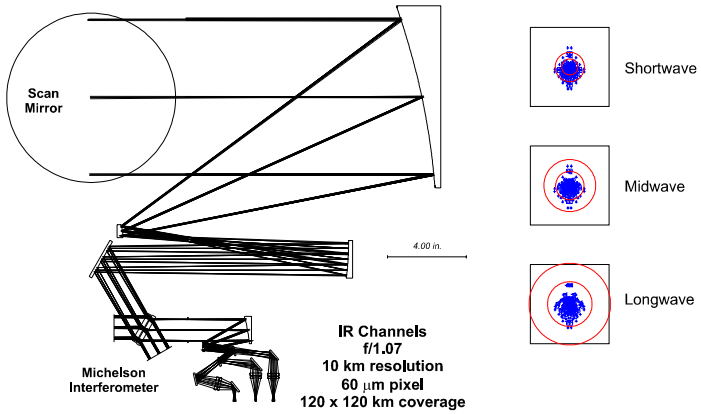

Figure 7. The optical layout of the ABS system is shown for the 20.3 cm aperture diameter.

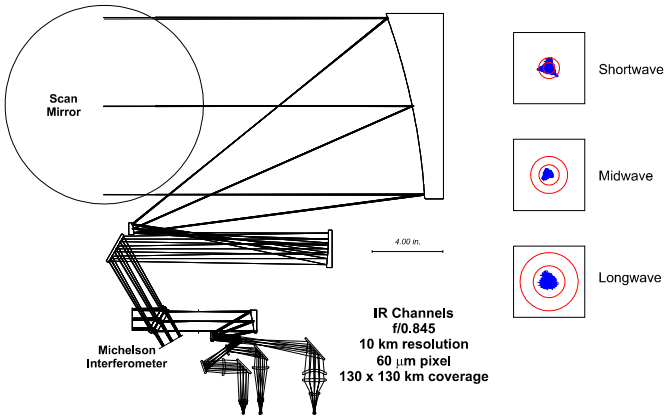

Figure 8. The optical layout of the ABS system is shown for the 25.4 cm aperture diameter.

Note that in the design shown in Figure 8, an extra refractive element was used in the back optics of each channel to obtain good optical performance.

3.2.2 Effect of Increased Aperture Diameter on ABS Volume, Mass, and Power

Increasing the ABS aperture diameter causes a proportional increase the volume and mass of the sensor. The scan mirror, telescope primary, and calibration blackbody become larger, as does the ambient-temperature optics bench. The sensor housing becomes larger as well. Figure 9 illustrates the estimated volume of the 15-cm system baselined in reference (1) along with the increase in volume anticipated as a result of moving to an 20-cm or 25-cm system with optics designs corresponding to Figures 6 through 8. Note that the assumption is made that the cooler area is unchanged because of the constraints imposed on page 7. For this reason, no adjustment is made to L2.

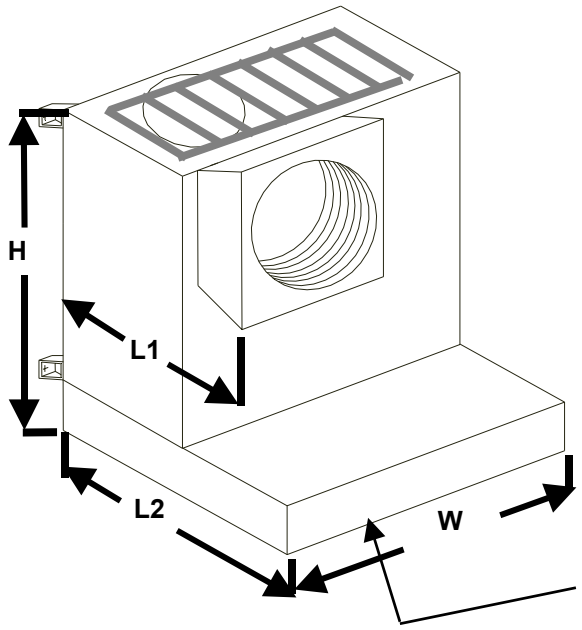

	Aperture Diameter		
	15.2 cm	20.3 cm	25.4 cm
L1 (cm)	43	53	64
L2 (cm)	58	58	58
H (cm)	66	71	79
W (cm)	61	71	76

Figure 9. The impact of changing the aperture diameter on the volume of the ABS sensor is illustrated. The figure is to scale for the 15-cm aperture.

Table 2 lists the corresponding mass information. The columns in Table 2 corresponding to 20-cm and 25-cm aperture diameters have been scaled from the 15-cm case for those components which are expected to become more massive in a larger-aperture design. The scaling of the optical bench, housing and louvres (assumed to cover the sensor housing opposite the radiative cooler) are determined from the dimensional changes implied by Figures 6 through 9. The mass of the louvres is modeled by assuming a density per unit area equivalent to 3.8 mm thick aluminum. The scan mirror mass, and the masses of the remaining optical elements are calculated using the optical design software. The blackbody and baffle mass were assumed to scale with the square of the diameter. The 25-cm aperture scan motor mass is taken from the ABI report. With the exception of the scan mirror, no lightweighting is assumed, and a 20% mass contingency is incorporated into the estimate.

TABLE 2

ABS Mass Estimate

	Mass (Kg)		
	15.2 cm Aperture	20.3 cm Aperture	25.4cm Aperture
Input aperture cover	-	-	-
Radiator cover	2.5	2.5	2.5
Optical bench (Al honeycomb)	6.2	8.9	11.1
IR cold bench	2.6	2.6	2.6
Passive thermal radiators	9.2	9.2	9.2
Moving-mirror assembly	2.3	2.3	2.3
Optics and supports	2.9	6.0	8.2
Scan mirror (Al 50% LW)	0.9	1.9	3.7
Scan motor ass'y & support	6.2	7.4	8.7
Blackbody calibration source	0.6	1.1	1.7
Housing (Al 1.5 mm thick)	5.7	7.0	8.4
Baffle	2.4	4.3	6.7
Radiation shielding	0.1	0.1	0.1
Magnetic shielding	0.6	0.7	0.8
Louvres (Al 3.8 mm thick)	2.0	2.7	3.4
Sensor estimate	**44.2**	**56.7**	**69.4**
Power supplies	6.0	6.0	6.0
Electronics	14.0	14.0	14.0
20% Contingency	12.8	15.3	17.9
ABS Total mass	**77**	**92**	**107**

The ~50% power savings projected for the 15-cm aperture ABS design over the filter-wheel sounder was largely due to the reduction in power needed for the scan motor. As the aperture diameter increases to approach that of the existing instrument, the power requirements of ABS would be expected to approach those of the filter-wheel sounder. The assumed material for the ABS scan mirror, however, was aluminum and the lightweighting assumed was a conservative 50%. While an aluminum scan mirror does not drive the mass estimate above, it has a much more profound impact on power consumption.

The power required to drive a scan mirror is proportional to the product of the mirror's rotational inertia and the angular acceleration during scanning. The angular acceleration of GOES I-M and ABS is roughly equal because the larger angular step of ABS is offset by its reduced scanning speed. The difference then comes down to rotational inertia, which is proportional to the fifth power of the aperture diameter. The factor of 32 savings in power consumption theoretically achievable by moving from the 30.5-cm GOES I-M aperture to a 15.2-cm ABS aperture was, in fact, assumed to be ~5 because of the choice of mirror material and lightweighting. The projected power consumption for the scan mirror, and for the ABS instrument, are shown in Table 3. As this table makes clear, the power consumption requirements implied by a larger aperture diameter would likely drive the scan mirror to the lightweighted beryllium construction currently used on the GOES imager and sounder instruments.

TABLE 3

ABS Power Consumption Estimate

Mirror material, and consumed power (W)	**15.2 cm Aperture**	**20.3 cm Aperture**	**25.4 cm Aperture**
Al, scan motor	12.5	53	161
Al, ABS system	**68**	**109**	**217**
Be, scan motor	-	11	32
Be, ABS system	-	**67**	**88**

3.2.3 Effect of Increased Aperture Diameter on ABS Detector Arrays and Radiometric Performance

This section examines the impact of increasing the ABS aperture diameter on the detector arrays and the system NEdN. The desired benefit is to improve the spatial response, while the constraints imposed are taken from page 7, and Sections 3.2.4 and 3.3. The end result is a design which meets the ensquared energy and NedN requirements while preserving single-readout operation of the FPA's.

Figure 10 is a reproduction of Fig. 4-35 in the ABS study report[1]. The dashed curve illustrates the need to read the longwave focal plane more rapidly as the aperture diameter increases to prevent the photocurrent (which increases with the photon flux entering ABS through a larger aperture) from overfilling the charge-storage capabilities of the readout. This charge-storage issue arises because the LW photodiodes require a small reverse-bias for impedance matching considerations, and the addition of the resulting dark current to the photocurrent stresses the charge-storage capacity available in silicon readout IC's. This topic is treated in detail in the ABS report.

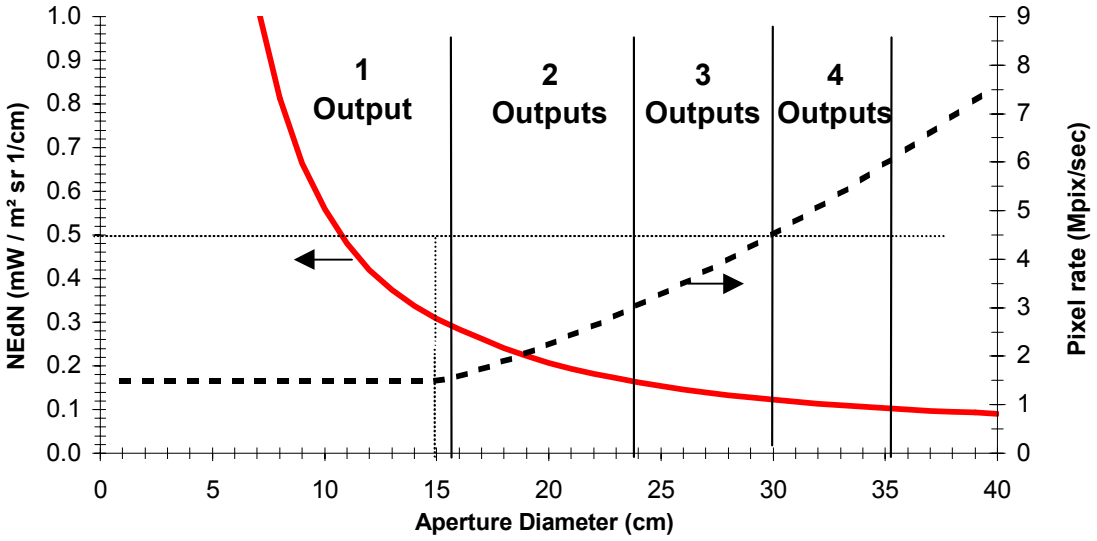

Figure 10. The NEdN and minimum pixel rate are illustrated for the 16x16 ABS LWIR array as a function of the aperture diameter. An operating temperature of 75 K is assumed. The required number of 1.5 Mpixel/s outputs required to support the pixel rate is illustrated as vertical bars.

Figure 10 also illustrates the improvement in NEdN which is gained by increasing the aperture diameter. The loss of signal accompanied by under-sizing the pixels as in Section 3.2.4, or by inserting

an LWIR apodizing filter as in Section 3.3 negates this expected improvement. Radiometric modeling[1] has indicated that the longwave channel requires a maximum NEdN of 0.5 mW/(m^2 sr cm^{-1}) to meet the ±1 K NWS threshold[5] for sounding retrieval accuracy.

The need to use a single FPA output requires that the detector array format must be reduced for larger apertures to remain compatible with the existing ABS passive cooler design. In order to verify that radiometric performance does not suffer, and to examine the effect of apodization, radiometric modeling was performed on six design options for ABS compatible with a single LWIR output: three aperture diameters (15 cm, 20 cm and 25 cm) and two apodization cases (unapodized, and apodization modeled as a 50% transmissive / 25% emissive surface at the aperture stop). The results of this modeling, summarized in Table 4 illustrate that different array sizes can be used which are compatible with single-output operation while meeting the NEdN requirement in the LW channel (< 0.5 mW/(m^2 sr cm^{-1})).

TABLE 4

FPA Readout Implications of Aperture Diameter Changes

	15.2 cm Aperture		20.3 cm Aperture		25.4 cm Aperture	
	Clear	Apod.	Clear	Apod.	Clear	Apod.
Effective *f* - number	1.42		1.07		0.86	
Photocurrent (10^{12} e^-/s)	1.10	0.70	2.00	1.20	3.10	1.90
Thermal current (10^{12} e^-/s)	0.51					
Max. integration time (μs)	170	232	112	160	77	115
Min. frame rate (kHz)	5.8	4.3	9.0	6.3	12.9	8.7
Array size	**16x16**	**18x18***	**12x12**	**15x15***	**10x10**	**13x13***

* The optics were designed for the array size specified for the *unapodized* case, except in the case of the 25-cm aperture which has been chosen as the new point design. Radiometric considerations alone allow for a 15x15 array size for a 25-cm aperture and LWIR apodizing filter if the detectors are undersized to 48 μm as recommended in Section 2, however the performance of the optical system may not be adequate for this wider field-of-view. It is for this reason that the array format is specified as 13x13 in Section 2.

3.2.4 Effect of Reduced Detector Pixel Size on ABS Detector Arrays and Radiometric Performance

Sections 3.2.1 and 3.2.3 have shown that an increased aperture diameter up to 25.4 cm may be implemented without major redesign of ABS. Referring to Figure 5 in Section 3.1, it can be seen that some reduction in the detector FOV (e.g. to 8 km) would produce a substantial benefit in ensquared energy in addition to that obtained with a larger aperture. As stated earlier, the GOES I-M sounder has a detector FOV smaller than the nominal 10-km resolution, partly because it's four ground FOV's are not contiguous. The implementation of a reduced 8-km detector geometry which preserves the spacing of the 10-km ground FOV's is illustrated in Figure 11.

[5] NWS Operational Requirements for Future Geostationary Operational Environmental Satellites (GOES), John J. Kelly, 8 January 1999.

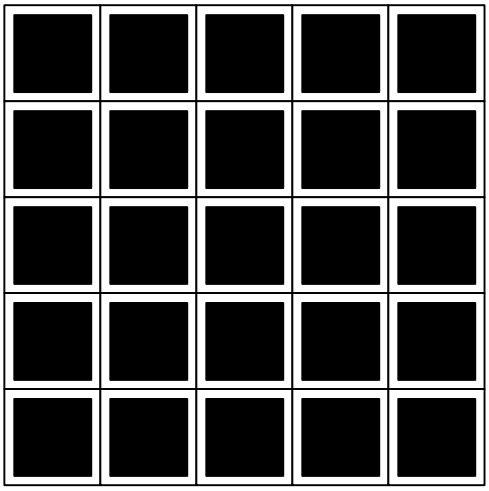

Figure 11. A focal plane is shown with 48 μm pixels on 60 μm centers.

A detector format such as the one shown in Figure 11 may be obtained by etching away the photosensitive material between the pixels, or by delineating a narrow trench around the pixels and grounding the photosensitive material between the pixels.

A negative effect associated with the use of a smaller detector size is that the NedN is increased because of the smaller signal flux captured by the detector pixel (note that a microlens array or other concentrator does not provide the necessary optical isolation). Detailed radiometric modeling of reduced-FOV detectors has been performed as necessary to support the point design of Section 2, and is incorporated into Figure 1.

A second undesired effect associated with the use of a smaller detector size is that the system spatial response becomes more sensitive to wavelength. Returning to Figure 3, it is clear that as the pixel FOV is reduced, the system spatial response goes from being dominated by the (wavelength-independent) pixel FOV to the (wavelength-dependent) diffraction spot size.

3.3 EFFECTS OF PUPIL APODIZATION ON ABS SPATIAL PERFORMANCE

The measures discussed in Section 3.2 are sufficient (in some combination) to equalize the spatial resolution of ABS to that of the GOES I-M sounder. The I-M sounder has some difficulty in obtaining clear-air soundings through "holes" in cloudy regions – even when they are sufficiently large that a geometric FOV is available which is free of cloud cover. While equalizing the ABS to the existing sounder is highly desirable, measures which might improve its ability to obtain soundings near cloud-covered areas over those of the existing instrument are likewise highly desirable. Returning to Figure 3 in Section 3.1, it can be seen that the 30-km width of the simulated cloud-free region should not cause radiometric error if the "spillover" of ensquared energy from the 10-km geometric FOV occurs only into adjacent pixels. As the figure makes clear, however, the spatial spread of energy (arising from diffraction) is sufficient to create a significant radiance error from the clouds well beyond the geometric FOV. This radiance error translates into errors in the retrieved temperature and humidity profiles from this region. In many instances the most valuable soundings are obtained near cloudy regions which are associated with severe weather, and so the impetus exists for rejecting energy from well outside the geometric FOV.

In this section, a method for rejecting this energy is proposed which may be optionally inserted into the ABS optical train. The method relies on smoothly tapering, or "apodizing", the illumination of the aperture, or equivalently, the illumination of an accessible pupil. The spatial filtering of the pupil illumination results in a decrease of the high-spatial-frequency content of the diffraction spot at the focal plane. It is this component of the diffraction spot which dominates the response far from the geometric FOV.

3.3.1 Selection of an Apodization Profile

Although the detailed design of the apodizing filter is not described here, it is assumed to be an IR window coated with a graded-density spectrally flat (neutral) coating. It would be placed at an image of the aperture within the optical train, two of which are present in the ABS optical design as shown in Figure 12. The first, just past the interferometer, is 2.8 cm in diameter and is common to all three IR bands. The second pupil location is present in the aft optics at the detector cold stops, and is ~ 0.3 cm in diameter. This second location allows an apodizing filter to be implemented in only the LW band, where diffraction is most prevalent.

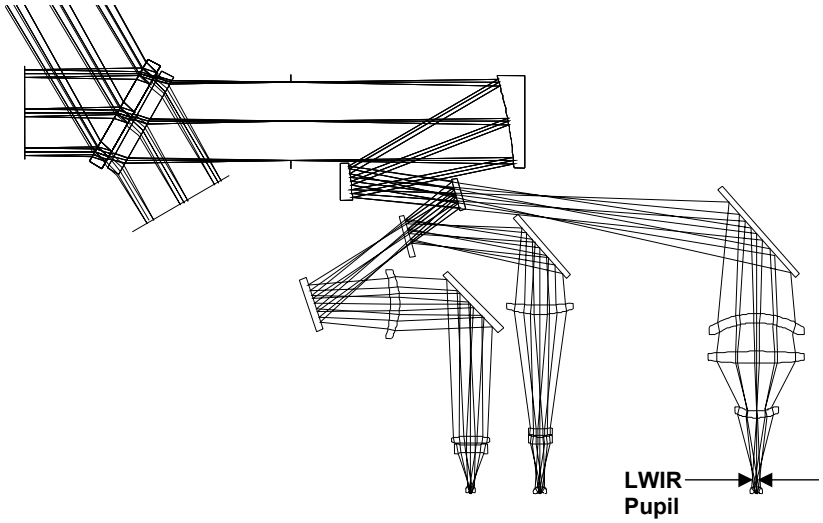

Figure 12. The location of the ABS point design LWIR pupil is illustrated.

There are several candidate apodization profiles available to reduce the subsidiary rings in the diffraction spot which contribute to contamination of soundings by energy from outside the geometric FOV. Investigation of these different profiles[6] concluded that a Gaussian, or modified Gaussian, profile provides the best combination of diffraction and attenuation properties. Two such profiles are shown in cross-section on the left side of Figure 13, while the resulting diffraction spot is shown on the right side of the figure. Note that the right side of Figure 13 plots the electric field magnitude (rather than the intensity) in order to accentuate the magnitude and location of the subsidiary diffraction maxima. In all cases, there is a reduction in the magnitude of the subsidiary maxima caused by removal of high-spatial-frequency content in the diffraction spot by the "smoothing" effect introduced by pupil apodization. Note that although all analysis in this section are for monochromatic radiation, the extension to the polychromatic case is straightforward.

[6] MIT/LL memorandum, "Apodization of ABS IR channels to reduce cloud contamination," Mike MacDonald, 4 January, 1999.

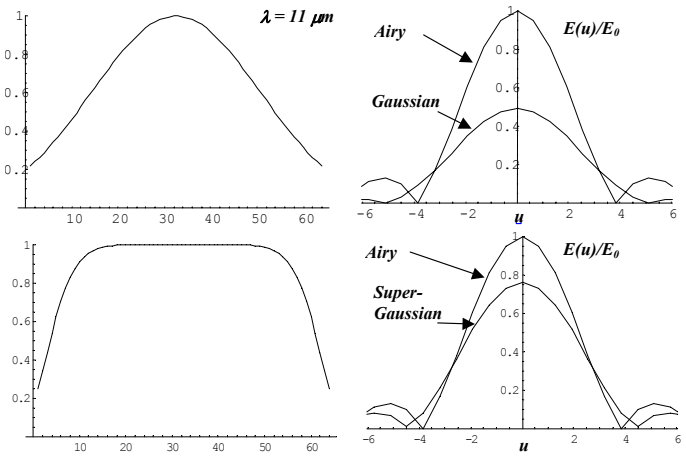

Figure 13. Two apodization profiles are shown at left. The corresponding diffraction spot (plotted as E field magnitude) are shown along with an unapodized spot for comparison at right.

This benefit does not come without cost, however – there is a reduction in the brightness of the diffraction spot, and a broadening of the width of the spot. Both of these effects are visible at the right side of Figure 12, and both occur because the concentration of energy in the center of the aperture reduces the "effective" aperture diameter.

Several Gaussian and linear apodizing profiles were modeled[7] for the 15-cm, 20-cm and 25-cm aperture diameters considered during the ABS work, and for the unobscured and obscured cases. A 25% obscuration was assumed when present (ABS was designed as an unobscured system, but the option of using a centered metrology system in the interferometer has remained open). Since a de-centered metrology system may be implemented (e.g. GHIS[8]) the unobscured option is preferred, and the modeling of an obscured system was largely for reference.

The benefit of apodization is primarily seen when considering the influx of energy into an FOV from FOV's which are not directly adjacent. This is very nearly eliminated in an apodized system, as illustrated in Figure 14. The gains in ensquared energy in the central FOV are rather modest, in large part because the diffraction spot is broadened somewhat, and the convolution of the FOV with the diffraction spot inherently leads to some spillage of energy into the adjacent FOV's. The reduction of signal flux by the filter varies with the profile used, but is generally about 50% for filters which provide the best spatial results. The intensity apodizing profile used was given by

$$I(r) = e^{-2(r/r_e)^k} \quad ; \quad 0 \le r \le r_a \tag{1}$$

with $k = 4$, and $r_e = 0.9\ r_a$. The remaining parameters assumed are those in Figure 5 for the 10-km FOV.

[7] MIT/LL Memorandum, "Optimal apodization profiles for the ABS instrument," M. E. MacDonald, 18 June, 1999.
[8] W. E. Bicknell, et. al., "GOES High-resolution interferometer sounder (GHIS) brassboard test program," MIT Lincoln Laboratory, Project Report NOAA-22, 22 July, 1998.

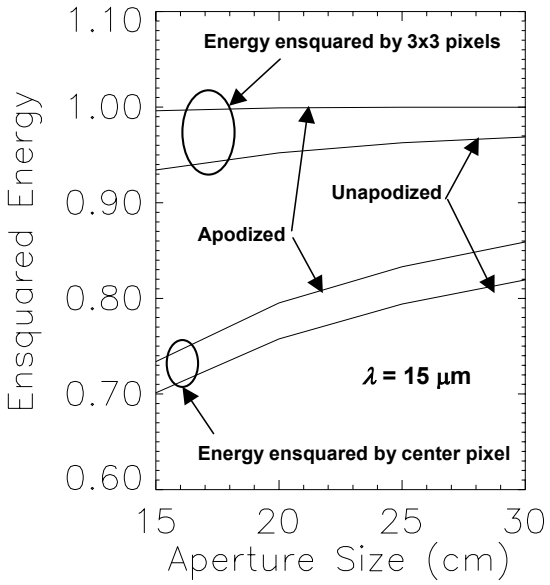

Figure 14. The energy ensquared by a single pixel, and by a square 3x3 array of pixels, is shown for the unapodized case, and for an equivalent apodized case.

Figure 15 illustrates how a 3x3 array of FOV's ensquare the energy originating from the central FOV for the unapodized and apodized (as in Figure 14) cases, and with and without reduced pixel fill factor. Again, there is a modest increase in the energy ensquared by the central FOV, and a modest reduction in the adjacent FOV's. Outside the central 3x3 FOV's, the optical crosstalk is virtually eliminated.

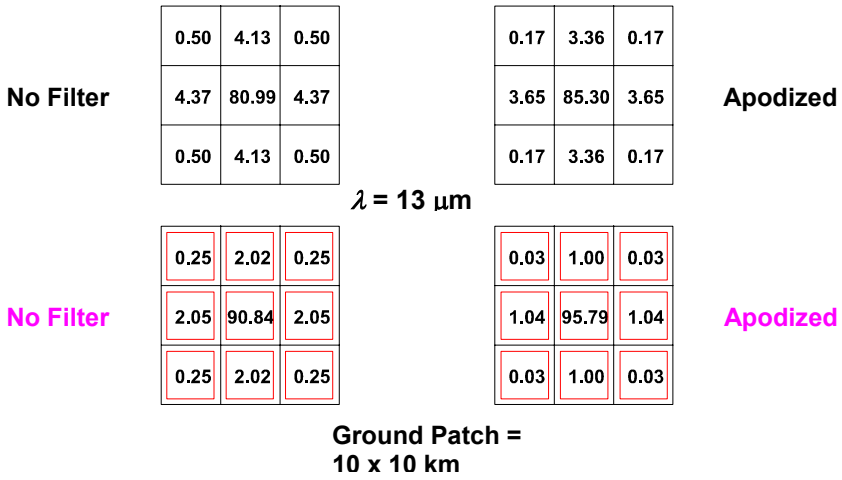

Figure 15 . The ensquared energy of the 25-cm aperture point design is shown with and without an apodizing filter, and with and without pixels undersized to 48 μm.

The effect of apodization on signal flux reaching the central FOV is to reduce it to approximately 50% of its unapodized value. The numbers in Figure 15 are expressed in terms of ensquared energy (see Appendix A), and do not reflect the relative signal changes imposed by apodizing and/or using a reduced pixel fill factor.

APPENDIX A

DEFINITION OF TERMS

Figure A1 illustrates the geometry considered in this document. An array of abutted square fields-of-view, each of which is to be sounded, is sampled using detectors which are undersized with respect to the FOV to improve the isolation between adjacent soundings. The left and right sides of Figure A1 are intended to illustrate the geometry relevant to the focal plane and the earth scene, respectively. The two sides are scaled by the ratio of the satellite altitude *H* and the ABS effective focal length *f*.

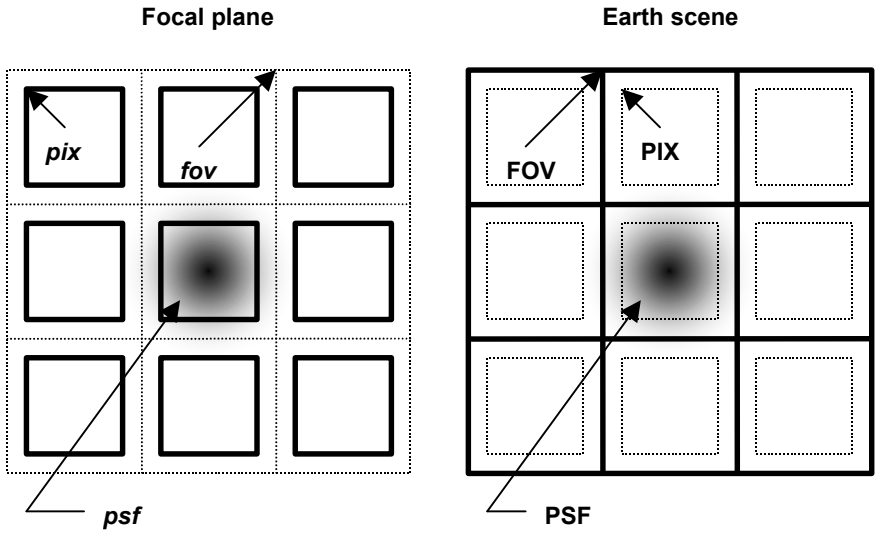

Figure A1. The geometry used to define the terms used in this document is illustrated.

The PSF undergoes the same scaling between the focal plane and the earth scene, however the geometry which it blurs by diffraction differs for these two cases – when we use scene coordinates the pixel geometry is blurred, while at the focal plane the scene FOV is blurred.

If we denote the focal-plane geometry of the pixel as *pix*, the geometric image of the FOV at the focal plane as *fov*, and the point-spread function as *psf*, we can then create a similar set of geometric objects at the earth scene, namely *PIX*, *FOV*, and *PSF* (capitalized as a reminder that they are magnified by the ratio *H*/*f*). These are illustrated in Figure A1.

For any detector pixel, and its corresponding FOV, we define ***spatial response*** as follows:

$$\textbf{\textit{spatial response}} \equiv PIX \otimes PSF \,. \tag{A1}$$

At the earth scene, this corresponds to the relative response of the instrument as a function of longitude and latitude. At the focal plane its analog, *pix* ⊗ *psf*, corresponds to a spot-scan of the detector.

We can define for the same pixel the ***ensquared energy***, as follows:

$$\textbf{ensquared energy} \equiv \frac{\iint_{sounded\ FOV} PIX \otimes PSF}{\iint_{all\ FOV's} PIX \otimes PSF}. \tag{A2}$$

At the earth scene, this corresponds to the spatial response, integrated over the FOV being sounded, divided by the spatial response integrated over infinity. Its focal plane analog,

$$\frac{\iint_{sounded\ pix} fov \otimes psf}{\sum_{\substack{all \\ pixels}} \iint_{pix} fov \otimes psf},$$

corresponds to the physical process of detection, and the summation is included to explicitly show that the energy falling between the pixels is not included in the denominator.

Finally, we define a quantity at the focal plane which we term ***relative signal*** which accounts for signal loss incurred by under-sizing the pixel:

$$\textbf{relative signal} \equiv \frac{\iint_{sounded\ pix} fov \otimes psf}{\iint_{sounded\ fov} fov \otimes psf}. \tag{A3a}$$

Although this term is defined above in terms of fill factor, it will also be used to account for energy loss due to apodization by a normalized illumination taper $I(r)$ at the pupil:

$$\textbf{relative signal} \equiv \frac{2\pi \int_{0}^{r_{pupil}} I(r) r dr}{\pi r_{pupil}^2}. \tag{A3b}$$